COMPLETE SPINAL CORD TRANSECTION TREATED BY IMPLANTATION OF A REINFORCED SYNTHETIC HYDROGEL CHANNEL RESULTS IN SYRINGOMYELIA AND CAUDAL MIGRATION OF THE ROSTRAL STUMP

Hiroshi Nomura, M.D., Ph.D.
Toronto Western Research Institute,
Toronto Western Hospital,
Toronto, Canada

Yusuke Katayama, M.A.Sc.
Matregen Corporation,
Toronto, Canada

Molly S. Shoichet, Ph.D.
Departments of Chemical Engineering
and Applied Chemistry
and Chemistry and Institute
of Biomaterials and Biomedical
Engineering,
Toronto, Canada

Charles H. Tator, M.D., Ph.D.
Toronto Western Research Institute,
Toronto Western Hospital,
University of Toronto,
Toronto, Canada

Reprint requests:
Charles H. Tator, M.D., Ph.D.,
Toronto Western Research Institute,
Toronto Western Hospital
and University of Toronto,
Room 2-435, McLaughlin Wing,
399 Bathurst Street,
Toronto, Ontario, Canada M5T 2S8.
Email: charles.tator@uhn.on.ca

Received, October 12, 2005.
Accepted, March 8, 2006.

OBJECTIVE: Previously, we reported that synthetic poly(2-hydroxyethyl methacrylate-co-methyl methacrylate) (PHEMA-MMA) channels promoted regeneration of a small number of axons from brainstem motor nuclei yet provided limited functional recovery after complete spinal cord transection at T8 in rats. However, we found that these modulus channels partially collapsed over time. Therefore, we synthesized coil-reinforced PHEMA or PHEMA-MMA channels with greater elastic moduli and introduced a new spinal fixation technique to prevent collapse. We also assessed axonal regeneration within the new channels containing a cocktail of autologous peripheral nerve grafts, fibrin matrix, and acidic fibroblast growth factor.

METHODS: After spinal cord transection, rats were divided into six groups: Groups 1 and 2 had either a PHEMA or PHEMA-MMA reinforced channel implanted between the stumps of the transected spinal cord with the cocktail; Groups 3 and 4 had either an unfilled reinforced PHEMA or PHEMA-MMA channel similarly implanted; Group 5 had an spinal cord transection without channel implanted, and Group 6 underwent the identical procedure to Group 1, but rats were sacrificed by 8 weeks for early histological assessment. Groups 1 to 5 were sacrificed at 18 weeks.

RESULTS: There was no channel collapse at any time. However, there was no improvement in axonal regeneration or functional recovery among Groups 1 to 4 because of the unexpected development of syringomyelia and caudal migration of the rostral stump. Functional recovery was better in Groups 1 to 4 compared with Group 5 ($P < 0.05$).

CONCLUSION: The use of channels to enhance regeneration of axons is promising; however, improvement of the design of the channels is required.

KEY WORDS: Axonal regeneration, Coil-reinforced nerve guidance channels, Peripheral nerve grafts, Poly(2-hydroxyethyl methacrylate-co-methyl methacrylate) channels, Spinal cord injury, Spinal cord transection, Syringomyelia

Neurosurgery 59:183-192, 2006 DOI: 10.1227/01.NEU.0000219859.35349.EF www.neurosurgery-online.com

The adult mammalian central nervous system (CNS) is unable to regenerate sufficient numbers of axons to allow significant functional recovery after major trauma (9). Necrosis and cystic cavitation contribute to the failure of axonal growth after CNS injury, particularly in adult spinal cord injury. One of the principal strategies to enhance regeneration is to bridge the injury site with scaffolds containing cells that promote axonal regrowth and reduce the barrier caused by scar tissue (28). Furthermore, combination strategies, such as peripheral nerve (PN) grafts and neurotrophic factors, may be more effective in enhancing axonal regeneration after spinal cord transection (SCT) (5, 22) than single strategies. Synthetic scaffolds have also been investigated as bridges between the stumps after SCT (7, 8). In particular, synthetic hydrogel scaffolds present many advantages for implantation because they can be designed with mechanical properties similar to those of the spinal cord and are permeable to nutrients and oxygen (11). Another advantage is that tubular scaffolds permit combination therapy, such as Schwann cells and neurotrophic factors, to enhance axonal regeneration (13, 14, 35).

Poly(2-hydroxyethyl methacrylate) (PHEMA) and poly(2-hydroxyethyl methacrylate-co-methyl methacrylate) (PHEMA-MMA) have been the most widely studied synthetic, nonbiodegradable hydrogels (16, 29, 32, 33). They are chemically stable, resistant to acid hydrolysis, biocompatible, and the elasticity can be modified by varying the amount of the cross-linking agent (29). Recently, we reported that PHEMA-MMA channels with an elastic modulus of 311 kPa promoted a small amount of axonal regeneration from brainstem motor nuclei in adult rats and enhanced functional recovery after complete SCT (32). However, in these initial studies, some of the PHEMA-MMA channels partially collapsed after implantation because of their low mechanical strength, and we questioned whether collapse compromised regeneration. The collapse was attributed to factors such as pressure from the adjacent paravertebral muscles. Although the PHEMA channels showed a similar tendency to collapse, PHEMA is less likely to calcify than PHEMA-MMA (21). Thus, in the present study, coil-reinforced PHEMA channels were compared with PHEMA-MMA channels for spinal cord repair. The objective was to determine whether the coiled guidance channels, which were approximately seven times stronger than the noncoiled channels previously used (20), would enhance axonal growth and functional recovery after SCT in the adult rat and also to examine the value of combination therapy with channels containing PN grafts and neurotrophic factors. To ensure patency of the implanted channels, we introduced a new method of spinal fixation.

MATERIALS AND METHODS

Production of Channels

PHEMA-MMA and PHEMA channels were prepared as previously described by Dalton et al. (11). Coil-reinforced channels were synthesized in cylindrical glass molds fitted with custom-made poly(ε-caprolactone) coils having a fiber diameter of 110 μm (*Fig. 1, A* and *B*). Before implantation, all channels were sterilized by gamma irradiation at 2.5 MRad. The length, outer and inner diameter, and the wall thickness of the channels were approximately 9.5, 4.0, 2.8, and 0.6 mm, respectively.

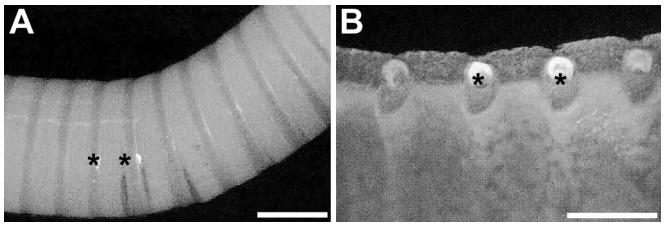

FIGURE 1. *Coiled synthetic hydrogel channel.* A, *external surface of PHEMA channel containing a condensed coil of the same material embedded in the wall of the channel.* Asterisks *indicate coils.* Scale bar, *2 mm.* B, *internal surface of the channel. Coils of condensed material are embedded in the wall of the channel.* Asterisks *indicate coils.* Scale bar, *660 μm.*

Animals

Adult female Sprague Dawley rats (200–320 g; Charles River, St. Constant, Canada) were used in this study. The animal protocols were approved by the Animal Care Committee of the Research Institute of the University Health Network in accordance with policies established by the Canadian Council on Animal Care. Sixty-seven rats with SCT were divided into six groups: Group 1 had implantation between the stumps of a coiled PHEMA channel containing 10 autologous intercostal nerve grafts and also received acidic fibroblast growth factor (aFGF) plus heparin in a fibrin matrix into the channel followed by spinal fusion (n = 12); Group 2 was identical to Group 1 except a coiled PHEMA-MMA channel was used instead of a coiled PHEMA channel (n = 12); Group 3 was identical to Group 1 except the coiled PHEMA channel was empty (n = 10); Group 4 was identical to Group 2 except the coiled PHEMA-MMA channel was empty (n = 10); Group 5 had complete SCT followed by spinal fusion but without implantation of a channel (n = 10); and Group 6 had 13 rats treated similarly to Group 1 but were sacrificed early for histological assessment at the following times: 1 week (n = 5), 2 weeks (n = 2), 4 weeks (n = 3), or 8 weeks (n = 3). The animals in Groups 1 to 5 were kept for 18 weeks after SCT. In summary, the combination therapy groups include Groups 1, 2, and 6, the empty channel groups include Groups 3 and 4, and the nonchannel control is Group 5.

Channel Implantation

Rats were deeply anesthetized with 2% halothane with 1:2 nitrous oxide to oxygen. In Groups 1, 2, and 6, the intercostal nerves from T6 to T10 were harvested bilaterally, and then the nerves were placed in Hank's buffered saline solution. After laminectomy from T7 to T9, the facets at the same levels were removed, the dura mater was longitudinally incised in the midline, and a synthetic expanded polytetrafluoroethylene membrane (preclude Dura Substitute Gore, gift from W.L. Gore & Associates, Inc., Flagstaff, AZ) was sutured to the left side of the durotomy with two 8–0 Vicryl sutures (Johnson & Johnson, Peterborough, Canada). The spinal cord at T9 was then completely transected with microscissors. The adjacent dorsal and ventral nerve roots were also completely transected to allow the stumps to be mobilized for insertion into the channels. An absorbable gelatin sponge (Surgifoam; Ethicon, Inc., Soeborg, Denmark) was placed between the two stumps to control hemorrhage. After removal of the gelatin sponge, the gap between the two stumps was approximately 2.5 mm (*Fig. 2A*). A V-shaped incision was made in the dorsal aspect of the coiled channels at both rostral and caudal ends to facilitate insertion of the stumps. In the combination therapy groups (Groups 1, 2, and 6), a bundle containing the harvested intercostal nerves was inserted into the channel. Then, the rostral cord stump was inserted approximately 3 mm into the rostral end of the channel. A combination of 0.075 μl of aFGF (Promega, Madison, WI) and 187.5 μl of heparin (Sigma, Oakville, Canada) were mixed with 30 μl of fibrin sealant

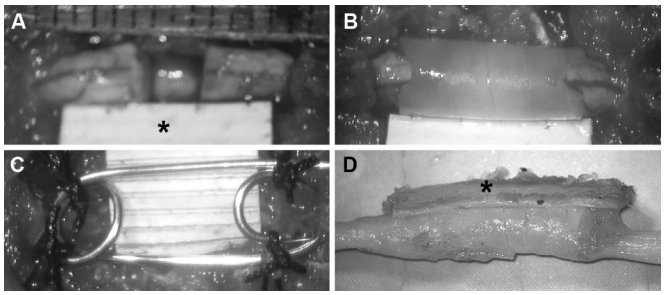

FIGURE 2. *Surgical procedure for PHEMA channel implantation* (A–C) *and gross appearance of the implanted channel at 18 weeks after channel implantation* (D). A, *complete transection of spinal cord at T8 and suturing of synthetic expanded polytetrafluoroethylene (ePTFE) membrane to left side of durotomy* (asterisk, *ePTFE membrane). Note that the gap between stumps of the transected spinal cord is approximately 3.5 mm in the rostrocaudal extent.* B, *implantation of the PHEMA channel with stumps placed inside.* C, *bilateral wire spinal fusion. The implanted channel is covered with ePTFE membrane.* D, *at 18 weeks, lateral view showing that there was no collapse of the channel* (asterisk, *ePTFE membrane).*

Beriplast P (Beriplast, gift from ZLB Behring GmbH, Marburg, Germany), which was then injected via a dual port micropipette into the caudal end of the channel. Then, the caudal stump was inserted approximately 3 mm into the caudal end of the channel (*Fig. 2B*). In all animals, the channel was positioned symmetrically so that equal lengths of rostral and caudal stumps were present in the channel; the remaining gap between the stumps in the channel was approximately 3.5 mm. The lamina at T6 and T10 prevented the channel from migrating rostrally or caudally after implantation. Then, 40 μl of Beriplast was applied to both the rostral and caudal stump-channel interfaces, and the dorsal aspect of the channel-stump construct was entirely covered by the Gore membrane. A spinal fusion was then performed from T6 to T10 with surgical wire and 2–0 silk so that there was a wire bridge along both the right and left dorsolateral aspects of the spinal cord (*Figs. 2C* and *3*). The incision was then closed with 3–0 Vicryl sutures in the paravertebral muscles and Michel clips (Fine Science tools, North Vancouver, Canada) in the skin. The methods for the empty channel groups (Groups 3 and 4) were identical except that the PN grafts, aFGF, and fibrin matrix were omitted. Group 5 had SCT only and did not receive PN grafts, aFGF, or fibrin matrix. Thus, spinal fusion was performed in all animals. All animals received buprenorphine (0.03 mg/kg) subcutaneously for 3 days postinjury, and manual bladder compression three times daily for the duration of the study.

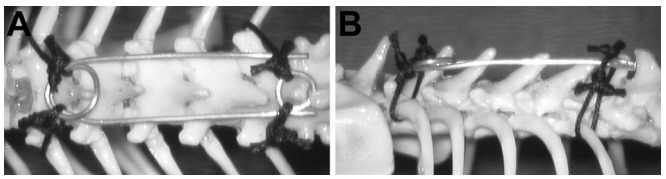

FIGURE 3. *New method of spinal fixation shown on skeleton of a rat thoracic spine showing sutures holding the wire in place.* A, *dorsal view.* B, *lateral view.*

Any urinary tract infection was treated with ampicillin (125 mg, every 12 h, subcutaneously) for 5 days.

Functional recovery was analyzed weekly during the 16-week survival period using the Basso, Beattie, Bresnahan (BBB) open field locomotor test (4). BBB scoring was conducted by three observers blinded to the experimental groups. All animals were scored and videotaped for 4 minutes every week for 16 weeks.

Tissue Preparation

To prepare tissues for paraffin embedding, rats were deeply anesthetized by an intraperitoneal injection of 1.0 ml of sodium pentobarbital. After an intracardiac injection of 1 ml of 1000 U/ml heparin, the animals were perfused through the ascending aorta with 500 ml of neutral buffered formalin. A 1.5- to 2-cm length of spinal cord centered on the site of transection and channel placement was carefully removed and postfixed in neutral buffered formalin. In Group 5, the 1.5- to 2-cm length of spinal cord that encompassed the transection site was harvested, preserving the tissue connecting the stumps of the spinal cord. After embedding in paraffin, 8-μm thick parasagittal sections were cut in a 1:8 series and mounted on Superfrosted Plus slides (Fisher Scientific, Markham, Canada). Every eighth section was stained with Luxol Fast Blue (LFB) with hematoxylin-eosin (H&E) to determine the series with the widest tissue bridge. Each section of that series was then stained with periodic acid Schiff in combination with LFB to distinguish peripheral from central myelin, the von Kossa silver stain for calcium, and prepared for immunohistochemistry as described below.

Immunohistochemistry of Paraffin-embedded Tissue

The following monoclonal antibodies were used for immunohistochemical assessment: mouse anti-neurofilament 200 antibody (NF200; 1:500 dilution, Sigma) to visualize neurons and axons; mouse anti-glial fibrillary acidic protein antibody (GFAP; 1:200 dilution; Boehringer-Mannheim Chemicon, Temecula, Canada) to visualize reactive astrocytes; mouse anti-microtube associated protein 2 antibody (MAP2; 1:1000 dilution, Chemicon) to visualize neurons and dendrites; mouse anti-rat P0 antibody (P0; 1:300, provided by Dr. Juan Archelos, Department of Neurology, University of Graz, Graz, Austria) to visualize peripheral myelin produced by Schwann cells (1, 19); mouse anti-rat monocytes/macrophages antibody (ED-1; 1:500, Serotec, Raleigh, NC) to visualize activated macrophages; and mouse anti-Ki67 liquid antibody (1:200; clone MM1, Novocastra, Burlington, ON, Canada) to visualize proliferating cells. In all these procedures, appropriate negative controls were used with the omission of the primary antibodies. The sections for GFAP, MAP2, and Ki67 were pretreated with 1% H_2O_2 in methanol for 30 minutes at room temperature (RT). The slides for MAP2 and Ki67 were placed in a pressure cooker with 3 g/L sodium citrate buffer (pH 6.0) and heated in a microwave (Kenmore Sears Canada, Inc., Toronto, Canada, model 88952) for 30 minutes on high power. After

heating, the slides were left in the microwave for another 30 minutes for cooling and were then rinsed with phosphate-buffered sodium (PBS) three times. For NF200, a plastic Coplin jar filled with a solution of ethylenediaminetetraacetic acid at pH 8.0 buffer was heated in a steamer (Black & Decker, Miami Lakes, FL) for 30 minutes. The slides were then placed in the ethylenediaminetetraacetic acid buffer in the Coplin jar and heated in the steamer for 30 minutes and were then left for 20 minutes for cooling. After having been rinsed with PBS, all sections except those for Ki67 were blocked for nonspecific antibody binding at RT for 1 hour with the following: 10% heat-inactivated goat serum in PBS containing 0.3% Triton X-100 for GFAP, NF200, and P0; 2% normal goat serum in PBS containing 0.3% Triton X-100 for MAP2 and 4% normal goat serum in PBS containing 0.1% Triton X for ED-1. The sections for Ki67 were blocked for nonspecific antibody at RT for 10 minutes with 2% normal horse serum in PBS containing 0.3% Triton X. Then, all sections except those for Ki67 were incubated overnight in a solution of primary antibody diluted in blocking solutions at 4°C. The primary antibody for Ki67 diluted in PBS was applied to the sections and then incubated at 4°C overnight. After being washed three times with PBS, the specimens were incubated with biotinylated anti-mouse immunoglobulin G (H+L) antibody (1:500 dilution in PBS; Vector, Burlingame, Canada). The sections were then washed three times in PBS and incubated with avidin-biotin peroxidase complex (Vectostain ABC Kit Standard; Vector Laboratories, Burlington, Canada) for peroxidase staining and visualization with diaminobenzidine tetrahydrochloride (Vector). The sections were cover-slipped with Entellan (EM Science, Gibbstown, NJ) and observed under a light microscope (Nikon Eclipse TE300; Nikon, Mississauga, Canada).

Anterograde Axonal Tracing of Corticospinal Tract with Biotin Dextran Amine

Four animals were randomly selected from each of Groups 1 to 5 for anterograde axonal tracing of the corticospinal tract with biotin dextran amine (BDA). BDA injection was performed 16 weeks after channel implantation. Under deep anesthesia, a craniotomy was performed to expose the sensorimotor cortex bilaterally, and 10% BDA (Molecular Probes Inc., Eugene, OR) dissolved in sterile distilled water was injected into 12 sites in each sensorimotor cortex with a glass micropipet attached to a 26 G needle and a Picospritzer, as previously described (34). At each coordinate, 2 μl of BDA was injected at a depth of 1.2 mm from the surface of the cortex. Animals were allowed to survive for 2 more weeks and then perfused with 500 ml of 4% paraformaldehyde in 0.1 mol/L PBS after an injection of heparin. A 1.5- to 2-cm length of spinal cord was harvested as described above. The spinal cords were immersed in chilled 30% sucrose in 0.1 mol/L PBS at 4°C and then frozen and embedded in Frozen Section Medium compound (Stephens Scientific, Riverdale, NJ). Twenty microliter thick parasagittal sections were cut serially on a cryostat and mounted on cold (−20°C) Superfrosted Plus slides (Erie Scientific, Portsmouth, NH). Every fourth slide was selected for BDA detection, and, after being washed with 0.1 mol/L PBS, these sections were pretreated with 1% H_2O_2 in methanol for 10 minutes at RT. After being rinsed with PBS containing 0.5% Triton X for 30 minutes, the slides were incubated in avidin-biotin peroxidase complex for 1 hour at RT. The slides were washed twice with PBS, and then Alexa Fluor 488 goat anti-mouse and goat anti-rabbit immunoglobulin G (H+L) conjugate highly cross-absorbed (1:500 dilution in PBS; Molecular Probes, Eugene, OR) were applied for 1 hour at RT. After being rinsed three times with PBS, the sections without cover-slipping were viewed with a fluorescent microscope.

Measurement of Length of Spinal Cord Stumps in Channels

For measurement of the length of the rostral and caudal stumps lying within the implanted channels at 18 weeks, the LFB/H&E parasagittal sections containing either the longest rostral or caudal stump were selected. The length of the implanted channel and the distances from the rostral or caudal ends of the channel to the tip of the rostral or caudal stumps, respectively, were measured using Bioquant Imaging Software (Nashville, TN) (*Fig. 4A*).

Measurements of Area of PN Grafts and Percent NF200 Area, Percent P0 Area, Percent Ki67 Area, and Percent ED-1 Area

For measurement of the area of the PN grafts in the channels in Groups 1, 2, and 6, each section containing the widest area of the PN grafts clearly surrounded by a membrane of epineurium was selected from all LFB/H&E sections at 1, 2, 4, 8, or 18 weeks after channel implantation. Only animals with remaining PN grafts entirely surrounded by epineurium were included in the analysis. Using an irregular region of interest, the entire area encompassed by the PN grafts was outlined and measured using Bioquant. For calculation of percent NF200 area, percent P0 area, percent Ki67 area, and percent ED-1 area in the PN grafts, the adjacent formalin fixed sections in the same series used for measurement of the area of the PN grafts were then stained for NF200, P0, Ki67, or ED-1, respectively. With use of an irregular region of interest, the area of the grafts labeled for each of these immunostains was measured using Bioquant, and then the entire area encompassed by them was also measured. Only areas of grafts surrounded by epineurium were used to calculate these percent areas. For all sections, the same light and threshold levels were maintained.

Statistics

The BBB scores of Groups 1 to 5 were analyzed by one-way analysis of variance, and the differences between two groups were analyzed by Mann-Whitney *t* test. Statistical analysis was performed using Sigma Plot 8.0 (StatSol, Saugus, MA) for Windows version and Microsoft Excel 2000 (Redmond, WA).

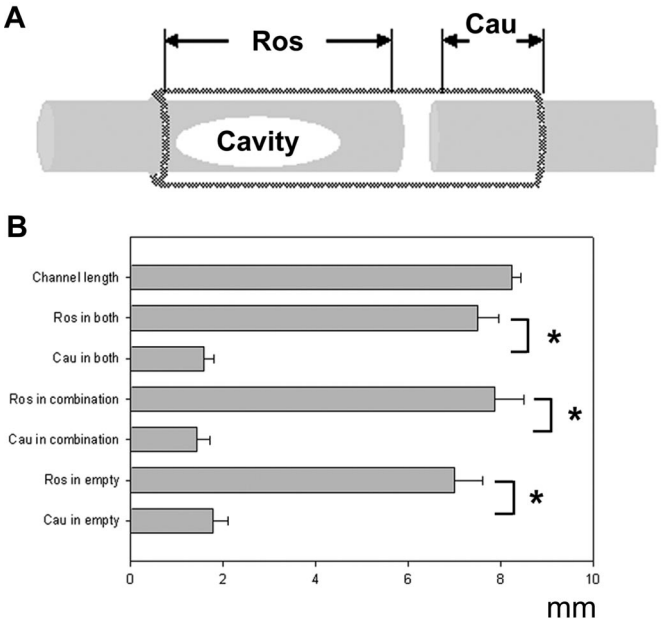

FIGURE 4. *Diagram* (A) *and bar graph* (B) *showing measurements of channel length and the length of the rostral and caudal stumps at 18 weeks after channel implantation in Groups 1 and 2 (n = 16) and Groups 3 and 4 (n = 12).* A, Ros *is the length of the rostral stump defined as the distance from the rostral end of the channel to tip of the rostral stump.* Cau *is the distance from the caudal end of the channel to the tip of the caudal stump.* B, *the first bar at the top of the graph shows that the mean length of the channels was 8.3 mm (range 6.1–10.0 mm). The rostral stump (mean, 7.8 mm; range 2.9–11.0 mm) was significantly longer than the caudal stump (mean, 1.7 mm; range 0–3.83 mm) in Groups 1 to 4 (*P *< 0.001). The rostral stump (mean, 8.6 mm; range 2.9–11.0 mm) was significantly longer than the caudal stump (mean, 1.5 mm; range 0–3.8 mm) in the combination therapy groups (*P *< 0.001). The rostral stump (mean, 7.1 mm; range 4.1–10.7 mm) was significantly longer than the caudal stump (mean, 1.9 mm; range, 0–3.1 mm) in the empty channel groups (*P *< 0.001). These data indicate that caudal migration of the rostral stump occurred in both the combination therapy and empty channel groups.*

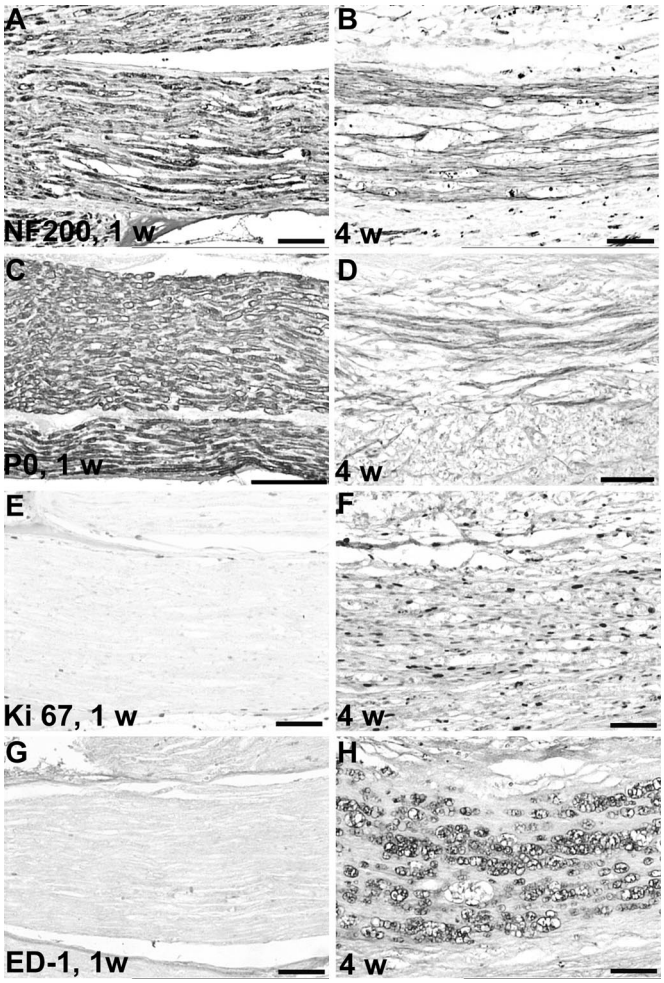

FIGURE 5. *Twenty micrometer parasagittal sections of PN grafts in a PHEMA channel at 1 week* (A, C, E, *and* G) *and 4 weeks* (B, D, F, *and* H) *after channel implantation. Immunostained with anti-NF200* (A *and* B), *P0* (C *and* D), *Ki67* (E *and* F), *and ED-1* (G *and* H) *antibody.* A, *a large number of NF200-positive axons is seen in the PN graft at 1 week.* B, *a major decrease in the number of NF200-positive axons is seen at 4 weeks compared with 1 week. Note that NF200-positive axons are severely degenerated.* C, *many P0-positive Schwann cells are seen in the PN graft at 1 week.* D, *small numbers of P0-positive Schwann cells are detected at 4 weeks.* E, *only few Ki67-positive cells are detectable at 1 week.* F, *many Ki67-positive Schwann cells are seen at 8 weeks.* G, *no ED-1-positive macrophages are observed at 1 week.* H, *large numbers of ED-1 positivemacrophages at 4 weeks.* A–H, *scale bar = 100 μm.*

RESULTS

Histological Examination

Early changes

At 1 week, the two stumps of the transected spinal cord and the implanted PN grafts were clearly observed in the channels. There was thickening of the arachnoid at both ends of the channels. Many NF200-positive axons and a large amount of P0-positive peripheral myelin were present in the grafts (*Fig. 5, A* and *C*), although only a small number of elongated Ki67-positive cells with spindle-shaped nuclei with the appearance of Schwann cells were found in the PN grafts (*Fig. 5E*). Accumulation of macrophages was not prominent in the grafts (*Fig. 5G*).

At 2 weeks, astrocytosis in a small area of both stumps was detected by GFAP immunostaining. Many ED–I-positive macrophages were detected in the PN grafts, especially adjacent to the stumps.

At 4 weeks, cavities had formed in the rostral and caudal stumps, but there was no obvious migration of the stumps. There was no evidence of direct connection between these cavities and the central canal, and no ependymal cells were found lining the wall of the cavities. Extensive arachnoid thickening was seen at both ends of the channels. The volume of the PN grafts declined progressively (*Fig. 6A*), there was a

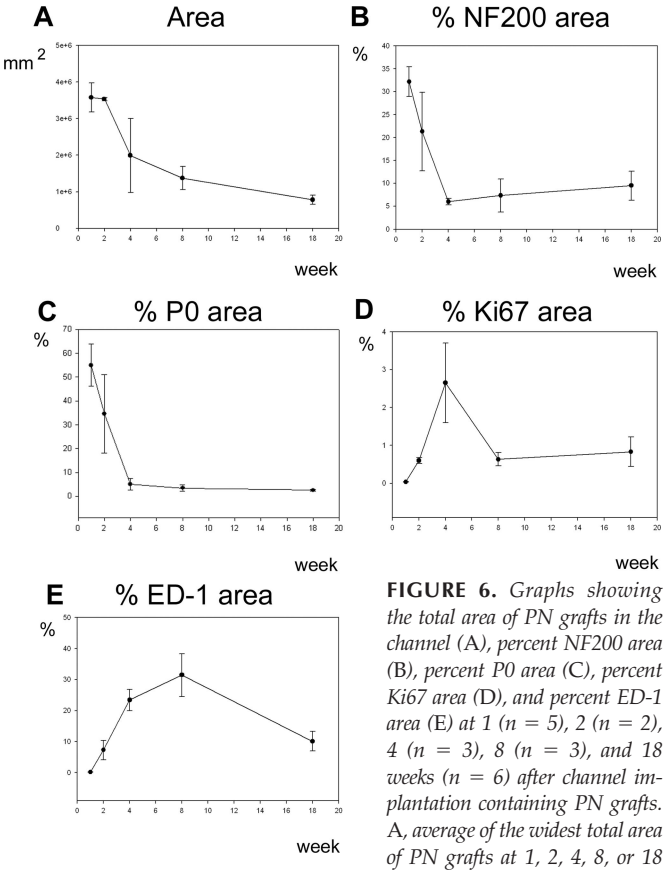

FIGURE 6. *Graphs showing the total area of PN grafts in the channel* (A)*, percent NF200 area* (B)*, percent P0 area* (C)*, percent Ki67 area* (D)*, and percent ED-1 area* (E) *at 1 (n = 5), 2 (n = 2), 4 (n = 3), 8 (n = 3), and 18 weeks (n = 6) after channel implantation containing PN grafts.* A*, average of the widest total area of PN grafts at 1, 2, 4, 8, or 18 weeks. Note that the area of PN grafts decreased over time.* B*, average percent NF200 area decreased between 1 and 4 weeks and then recovered slightly.* C*, average percent P0 area decreased severely between 1 and 4 weeks.* D*, average percent Ki67 area increased until 4 weeks and then decreased.* E*, average percent ED-1 area increased dramatically until 8 weeks.*

severe decrease in both NF200 (*Figs. 5* and *6B*) and P0 immunoreactivity (*Figs. 5* and *6, C* and *D*), and the remaining axons in the grafts were severely degenerated. Remarkably, many Ki67-positive Schwann cells were seen in the PN grafts at this time (*Figs. 5F* and *6D*), and very large deposits of ED–1-positive macrophages were also detected in the grafts (*Figs. 5* and *6, E* and *H*). At 8 weeks, caudal migration of the rostral stump was associated with an increase in size of the syringomyelic cavities.

Late Changes

At 18 weeks, all of the implanted channels remained patent on gross inspection (*Fig. 2D*), and LFB/ H&E-stained sections confirmed that the diameter of the inner lumen of the channels was maintained (*Fig. 7A*). However, almost all channels showed some inward extrusion of the coils from the walls of the channels, although none of the coils extruded sufficiently far to penetrate into the spinal cord. There was occasional minimal compression of the cord by an excluded coil (*Fig. 7B*). The von Kossa silver stain revealed calcification along the inner wall of the PHEMA and PHEMA-MMA channels at 18 weeks, with the amount of calcification of the PHEMA channels slightly lower than that of the PHEMA-MMA channels.

The rostral stump of the spinal cord had migrated within the channels toward the caudal stump in 26 of the 28 animals at 18 weeks (*Fig. 7A*). Moreover, there was a long syringomyelic cavity in the migrated rostral stump in 25 of the 26 animals. There was marked arachnoid thickening at the rostral end of the channels. There were identifiable ependymal cells in the stumps adjacent to the tissue bridge. However, there were only a few identifiable ependymal cells lining the wall of the syringomyelic cavities, and most of the lining cells were flattened, elongated cells resembling fibroblasts or Schwann cells. No direct connection between the syringomyelic cavities and the central canal was observed. In a small number of animals, there was an expansion of the central canal in the rostral stump. In 15 of the 26 animals, the elongating rostral stump directly contacted the caudal stump with no intervening tissue bridge. GFAP immunostaining showed a dense accumulation of astrocytes in both rostral and caudal stumps (*Fig. 7C*). A small number of NF200-positive axons were detected in the bridge between the stumps (*Fig. 7D*). Also, there was some peripheral myelin likely produced by Schwann cells immunolabeled with P0 in the bridge between the stumps (*Fig. 7E*). MAP2 immunostaining demonstrated many persisting and intact neurons and their dendrites in the migrating stump (*Fig. 7F*). Schwann cells were identified in the stumps and bridges not only in Groups 1 and 2 containing PN tissue/ aFGF, but also in the empty channel Groups 3 and 4. P0 immunostaining revealed a small amount of peripheral myelin in the migrating stumps and bridge in Groups 3 and 4. Significant aggregations of activated macrophages were observed in the spinal cord stumps by ED-1 immunostaining (*Fig. 7G*). There were no differences in the histology of the stumps or bridges between the combination therapy groups and the empty channel groups except for the infrequent presence of the PN grafts. In Groups 1 and 2, the PN grafts were atrophic, although aggregates of Schwann cells and myelin sheaths were present in the space between the stumps and the adjacent inner walls of the channels with NF200-positive axons (*Fig. 7H*), a small amount of P0-positive peripheral myelin (*Fig. 7I*), and a small number of Ki67-positive Schwann cells. None of these structures was present in the empty channel groups.

At 18 weeks in Group 5, there was thick, fibrous connective tissue between the stumps and cavitation in both stumps (*Fig. 7J*). This connective tissue did not contain NF200-positive structures or migrating Schwann cells.

Measurement of Caudal Migration and Syringomyelic Cavitation of Rostral Stump

As noted above, the majority of rats in Groups 1 to 4 had caudal migration and syringomyelia of the rostral stump at 18 weeks. In contrast, there was no instance of rostral migration of the caudal stump within the channel. To assess the extent of migration, the shortest distance from the rostral or caudal end

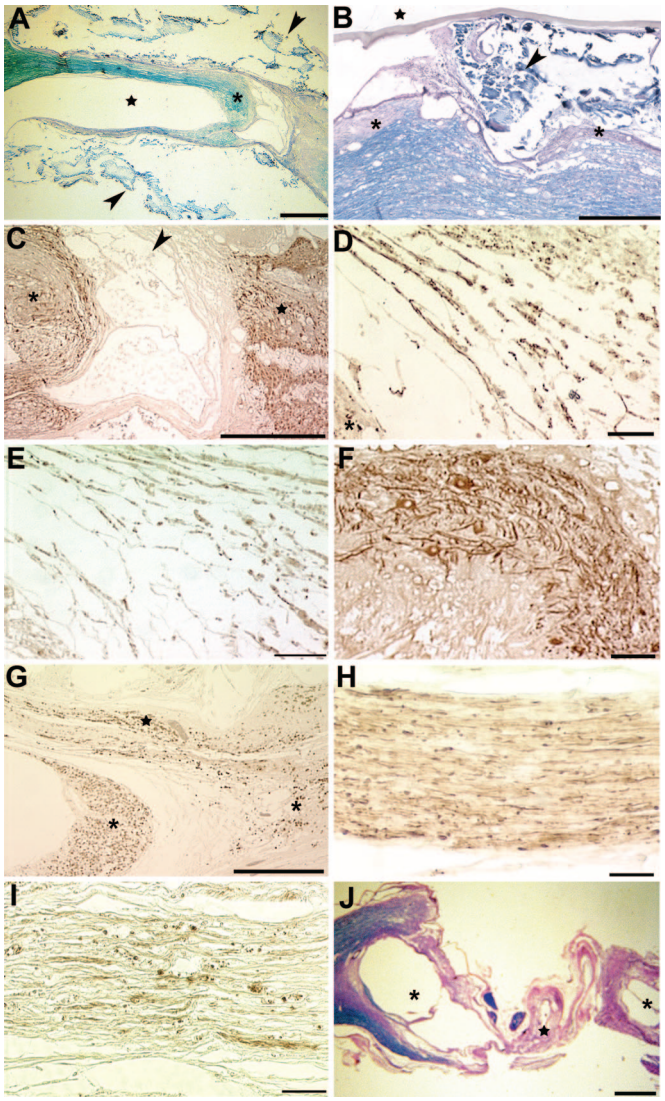

FIGURE 7. *Twenty micrometer parasagittal sections at 18 weeks after channel implantation. The following examples are shown: Group 1, rat containing PHEMA channel and combination therapy with PN grafts and aFGF in fibrin glue* (A, C, *and* F)*; Group 2, rat showing PHEMA-MMA channel with combination therapy* (D, E, G, H, *and* I)*; Group 4, rat with empty PHEMA-MMA channel* (B)*, and Group 5, rat with SCT without channel implantation* (J)*. In each example, the rostral is on the left.* A, *LFB/H&E stained section shows caudal migration of the rostral stump of the transected spinal cord* (asterisk) *associated with a large syringomyelic cavity* (star) *in the stump within the channel* (arrowheads *point to channel wall).* B, *LFB/H&E stained section showing inward extrusion of coils from the walls of the channels with minimal compression of the cord* (arrowhead) *and massive arachnoid thickening* (asterisk) *at the rostral end of the channel* (star *indicates Gore-Tex membrane).* C, *GFAP immunostained section of both stumps in the channel showing a distinct margin between the tissue bridge* (arrow) *and the rostral* (asterisk) *or caudal* (star) *stump caused by massive astrocytosis in the stumps. NF200* (D) *and P0* (E) *immunostained sections of bridge between stumps of transected spinal cord in channel; small number of NF200-positive axons are seen in the bridge* (asterisk, *portion of rostral stump in* D). E, *some peripheral myelin immunolabeled with P0 are present in the bridge.* F, *MAP2 immunostained section of rostral stump in channel showing many neurons and their dendrites.* G, *ED-1 immunostained section showing both stumps and PN grafts in the channel; massive aggregations of ED-1-positive macrophages are present in the spinal cord stumps* (asterisk) *and PN grafts* (star). H, *NF200 immunostained section of PN grafts in the channel showing some NF200 positive axons in graft.* I, *P0 immunostained section of PN graft in the channel showing some P0-positive Schwann cells.* J, *parasagittal section of STC without channel implantation in Group 5; thick scar tissue is present in gap between the stumps* (star). *Note the large cavities in both stumps* (asterisk). *Scale bars:* A *and* J, *1 mm;* B, C, *and* G, *0.5 mm;* D, E, *and* F, *100 μm;* H *and* I, *50 μm.*

of the channel to the tip of the rostral or caudal stump, respectively, was measured (*Fig. 4*). The mean length of the rostral stump in Groups 1 to 4 (n = 28) was 7.8 mm. In the combination therapy groups 1 and 2 (n = 16) and empty channel Groups 3 and 4 (n = 12), the mean lengths were 8.6 and 7.1 mm, respectively. In contrast, the length of the caudal stump in Groups 1 to 4 was 1.7 mm, in Groups 1 and 2 it was 1.5 mm, and in Groups 3 and 4 it was 1.9 mm. Thus, the length of the rostral stump was significantly longer than that of the caudal stump in Groups 1 to 4 (each $P < 0.001$) (*Fig. 4*).

Anterograde Axonal Tracing

The parasagittal sections were examined for BDA-labeled corticospinal tract fibers in the stumps and bridging tissue. Only BDA-positive structures demonstrating linear features were considered to be axons. In all groups, BDA-labeled fibers were detected in the rostral stump of the spinal cord although not all the way to the end of the stump. However, there were no BDA-labeled fibers caudal to the transection site in the bridging tissue or in the caudal stump (data not shown).

Functional Evaluation

At 16 weeks after surgical treatment, the BBB score of each treatment group (Groups 1–4) was significantly higher than that of the transection control group (Group 5), ($P < 0.05$) (*Fig. 8*). However, there was no significant difference in the BBB score among Groups 1 to 4 ($P = 0.516$).

DISCUSSION

Previously, we showed that empty synthetic hydrogel guidance channels composed of PHEMA-MMA supported axonal regeneration after SCT (32), and that PHEMA-MMA channels with an elastic modulus of 311 kPa promoted thicker bridging tissue containing more regenerating axons in the gap between the stumps compared with 177 kPa channels. Although the 311 kPa channels showed better regenerative capacity, the number of regenerating axons was still small, and the channels were not sufficiently strong to prevent partial collapse within 8 weeks of implantation. It is important to note that, in the previous study, there was no syringomyelic cavitation or

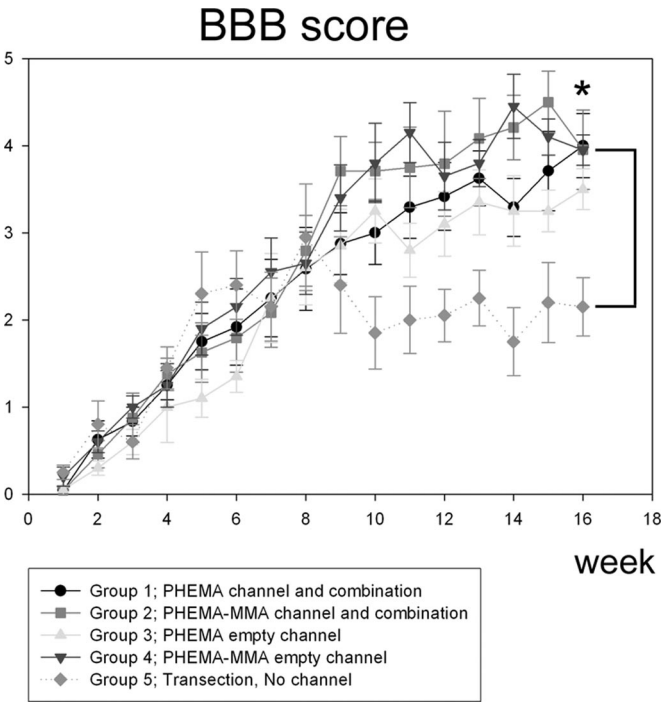

FIGURE 8. *Functional evaluation using the BBB score from 1 to 16 weeks after SCT and treatment in Groups 1 to 5. At 16 weeks after channel implantation or transection, the BBB score of each channel implantation group (Group 1, 2, 3, or 4) was significantly higher than that of the transection control group (Group 5) ($P < 0.005$), but there was no significant difference in BBB score among the four treatment groups at 16 weeks (one-way analysis of variance, $P = 0.516$).*

caudal migration of the rostral stumps. In the present study, the channels were reinforced by a coil embedded in the walls that made them approximately seven times stronger as measured by compression (20). The present study also introduced a new method of spinal fixation designed to prevent compression and subsequent collapse of the channels from pressure by the adjacent paravertebral muscles, an improvement over the fixation technique originally described by Cheng et al. (10) that provided only unilateral wire bridging of the laminectomy site. With the combination of coiled channels and bilateral wiring, the channels remained patent for the 18 week duration of the study. However, despite overcoming what we had thought was a physical barrier to regeneration, we did not improve axonal regeneration between the stumps compared with our previous work.

The bridging tissue in the gap between the stumps contained Schwann cells associated with axons in both the combination therapy and empty channel groups. Therefore, it is likely that some of the Schwann cells migrated into the bridge from the adjacent nerve roots and did not originate solely from the PN grafts. Others have reported that Schwann cells can support regeneration of CNS axons in spinal cord injury (2, 8, 27). Surprisingly, at 18 weeks, we did not see more Schwann cells in the bridges in Groups 1 and 2, the combination therapy groups, than in the empty channel groups, and there was only a small amount of P0-immunopositive peripheral myelin produced by Schwann cells remaining in the PN grafts. Importantly, we found no definite evidence that Schwann cells from the PN grafts had migrated into the cut ends of the transected spinal cord. Iwashita et al. (17) also found that transplanted Schwann cells did not migrate extensively into the spinal cord and showed poor long-term survival rates when introduced into a normal CNS environment, which is consistent with our findings. Thus, this method of transplanting Schwann cells resulted in poor transplant survival and bridging.

In contrast, it has been reported that PN grafts and aFGF in fibrin glue can enhance the regeneration of axons across the transected spinal cord (10, 22). We combined heparin with aFGF in fibrin to increase the activity of aFGF (15, 26) but found no difference in functional recovery between the combination therapy and empty channel groups, and bridging tissue was minimal in both groups. We also examined the sequence of histological changes in the grafted PNs and found major atrophy of the grafts associated with extensive aggregation of macrophages. By 18 weeks, most of the PN grafts had disappeared from the channels in the combination therapy groups, and many macrophages were still present. These findings indicate that phagocytosis by activated macrophages contributes to the destruction of the autologous grafts in a time-dependent manner.

The difference between our present study and the previous study in which some axonal regeneration was seen may be related to the fact that the stronger, noncollapsing coiled channels supported syringomyelic cavitation and caudal migration of the rostral stump, which may have prevented axonal regeneration. This unexpected occurrence of caudal migration and syringomyelic cyst formation in the rostral stump was not observed in the previous study. To our knowledge, this is the first report of caudal migration of the rostral stump caused by syringomyelia after SCT, and we hypothesize the following mechanisms: 1) first, syringomyelia occurs in the rostral stump in the first 4 weeks after SCT likely because of arachnoiditis and occlusion of the subarachnoid space, possibly aided coil extrusion (*Fig. 7B*); 2) the rostral stump then migrates toward the caudal stump through the channel as a result of the continuing expansion of the syringomyelic cavitation and possibly facilitated by the root transection described in Methods (*Fig. 9*). Obstruction of the subarachnoid space is considered to be an important mechanism in the pathophysiology of syringomyelia, as noted below. We found no evidence for rostral migration of the channel, probably because the channels were prevented from migrating rostrally because they abutted directly against the intact lamina rostral to the SCT. The findings in the present study indicate that future attempts to use the channel implantation strategy for the completely transected spinal cord should use larger diameter channels to avoid cerebrospinal fluid obstruction and subsequent syringomyelia.

Commonly, the cysts of syringomyelia have been classified into three types: communicating central canal syringes, non-

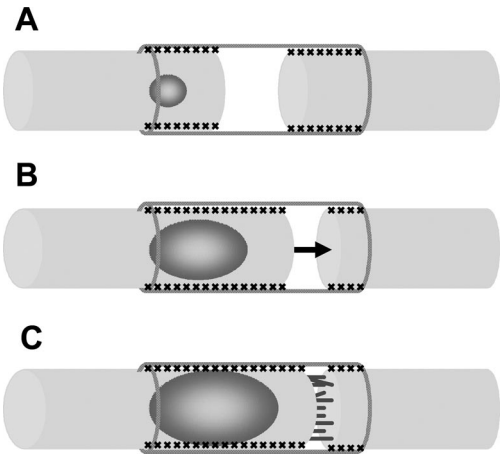

FIGURE 9. *Diagrams showing the mechanism of caudal migration of the rostral stump in the channel. In each diagram, the rostral side is on the left.* A, *the first cyst formation occurs in the rostral stump in the first 4 weeks after spinal cord transection because of the development of progressive syringomyelia.* B, *the rostral stump migrates toward the caudal stump.* C, *after regenerating axons, migrating Schwann cells and proliferating ependymal cells contribute to bridging the gap between the stumps.*

communicating central canal syringes, and extracanalicular syringes (23, 31). We found rare instances of a few ependymal cells lining the walls of smaller cysts in the stumps communicating with the central canal but no direct connection between the large cysts and the central canal. Thus, in the current study, we found a combination of communicating and extracanalicular syringomyelia, which is common in posttraumatic syringomyelia. Although the exact pathophysiology of posttraumatic syringomyelia is still unclear, many previous experiments have suggested that the entry of cerebrospinal fluid from the subarachnoid space into the primary cavity in the injured spinal cord is through the perivascular channels, the Virchow-Robin spaces, because of an obstruction of the cerebrospinal fluid in the subarachnoid space (3). After spinal cord injury, the subarachnoid space can become obstructed because of swelling of the cord, arachnoiditis from subarachnoid blood, and tethering of the cord to the dura. These mechanisms contribute to the development of posttraumatic syringomyelia (3, 6, 12, 18, 24, 25, 30).

Although the combination strategy with the PN grafts and aFGF was not more effective than empty channels, all the groups with implanted channels had higher functional recovery than the control group without channel implantation. Thus, the channels may have acted as a guide to maintain alignment and may have contributed to the presence of some of regenerating axons in the bridge between the stumps. Further design improvement of the channels is required and is ongoing to enhance axonal regeneration in the spinal cord.

REFERENCES

1. Archelos JJ, Roggenbuck K, Schneider-Schaulies J, Toyka KV, Hartung HP: Detection and quantification of antibodies to the extracellular domain of P0 during experimental allergic neuritis. **J Neurol Sci** 117:197–205, 1993.
2. Azanchi R, Bernal G, Gupta R, Keirstead HS: Combined demyelination plus Schwann cell transplantation therapy increases spread of cells and axonal regeneration following contusion injury. **J Neurotrauma** 21:775–788, 2004.
3. Ball MJ, Dayan AD: Pathogenesis of syringomyelia. **Lancet** 2:799–801, 1972.
4. Basso DM, Beattie MS, Bresnahan JC: A sensitive and reliable locomotor rating scale for open field testing in rats. **J Neurotrauma** 12:1–21, 1995.
5. Bregman BS, Coumans JV, Dai HN, Kuhn PL, Lynskey J, McAtee M, Sandhu F: Transplants and neurotrophic factors increase regeneration and recovery of function after spinal cord injury. **Prog Brain Res** 137:257–273, 2002.
6. Brodbelt AR, Stoodley MA, Watling A, Rogan C, Tu J, Brown CJ, Burke S, Jones NR: The role of excitotoxic injury in post-traumatic syringomyelia. **J Neurotrauma** 20:883–893, 2003.
7. Bunge MB: Bridging areas of injury in the spinal cord. **Neuroscientist** 7:325–339, 2001.
8. Bunge MB: Bridging the transected or contused adult rat spinal cord with Schwann cell and olfactory ensheathing glia transplants. **Prog Brain Res** 137:275–282, 2002.
9. Cajal YR: *Degeneration and Regeneration of the Nervous System*. New York, Oxford University Press, 1928.
10. Cheng H, Cao Y, Olson L: Spinal cord repair in adult paraplegic rats: Partial restoration of hind limb function. **Science** 273:510–513, 1996.
11. Dalton PD, Flynn L, Shoichet MS: Manufacture of poly(2-hydroxyethyl methacrylate-co-methyl methacrylate) hydrogel tubes for use as nerve guidance channels. **Biomaterials** 23:3843–3851, 2002.
12. Durward QJ, Rice GP, Ball MJ, Gilbert JJ, Kaufmann JC: Selective spinal cordectomy: Clinicopathological correlation. **J Neurosurg** 56:359–367, 1982.
13. Fouad K, Schnell L, Bunge MB, Schwab ME, Liebscher T, Pearse DD: Combining Schwann cell bridges and olfactory-ensheathing glia grafts with chondroitinase promotes locomotor recovery after complete transection of the spinal cord. **J Neurosci** 25:1169–1178, 2005.
14. Gautier SE, Oudega M, Fragoso M, Chapon P, Plant GW, Bunge MB, Parel JM: Poly(alpha-hydroxyacids) for application in the spinal cord: Resorbability and biocompatibility with adult rat Schwann cells and spinal cord. **J Biomed Mater Res** 42:642–654, 1998.
15. Guest JD, Hesse D, Schnell L, Schwab ME, Bunge MB, Bunge RP: Influence of IN-1 antibody and acidic FGF-fibrin glue on the response of injured corticospinal tract axons to human Schwann cell grafts. **J Neurosci Res** 50:888–905, 1997.
16. Gursel I, Balcik C, Arica Y, Akkus O, Akkas N, Hasirci V: Synthesis and mechanical properties of interpenetrating networks of polyhydroxybutyrate-co-hydroxyvalerate and polyhydroxyethyl methacrylate. **Biomaterials** 19:1137–1143, 1998.
17. Iwashita Y, Fawcett JW, Crang AJ, Franklin RJ, Blakemore WF: Schwann cells transplanted into normal and X-irradiated adult white matter do not migrate extensively and show poor long-term survival. **Exp Neurol** 164:292–302, 2000.
18. Josephson A, Greitz D, Klason T, Olson L, Spenger C: A spinal thecal sac constriction model supports the theory that induced pressure gradients in the cord cause edema and cyst formation. **Neurosurgery** 48:636–645, 2001.
19. Kamada T, Koda M, Dezawa M, Yoshinaga K, Hashimoto M, Koshizuka S, Nishio Y, Moriya H, Yamazaki M: Transplantation of bone marrow stromal cell-derived Schwann cells promotes axonal regeneration and functional recovery after complete transection of adult rat spinal cord. **J Neuropathol Exp Neurol** 64:37–45, 2005.
20. Katayama Y, Montenegro R, Freier T, Midha R, Belkas J, Shoichet MS: Coil-reinforced hydrogel tubes promote nerve regeneration equivalent to that of nerve autografts. **Biomaterials** 27:505–518, 2005.
21. Kim YH, Cho YS, Kim HW: Effects of methyl methacrylate on Ca2+ uptake of cardiac sarcoplasmic reticulum. **Pharmacol Res** 47:11–16, 2003.
22. Lee YS, Lin CY, Robertson RT, Hsiao I, Lin VW: Motor recovery and anatomical evidence of axonal regrowth in spinal cord-repaired adult rats. **J Neuropathol Exp Neurol** 63:233–245, 2004.
23. Milhorat TH, Capocelli AL Jr, Anzil AP, Kotzen RM, Milhorat RH: Pathological basis of spinal cord cavitation in syringomyelia: Analysis of 105 autopsy cases. **J Neurosurg** 82:802–812, 1995.
24. Milhorat TH, Nobandegani F, Miller JI, Rao C: Noncommunicating syringomyelia following occlusion of central canal in rats. Experimental model and histological findings. **J Neurosurg** 78:274–279, 1993.
25. Oldfield EH: Syringomyelia. **J Neurosurg** 95 [Suppl 1]:153–155, 2001.

26. Ornitz DM, Herr AB, Nilsson M, Westman J, Svahn CM, Waksman G: FGF binding and FGF receptor activation by synthetic heparan-derived di- and trisaccharides. **Science** 268:432–436, 1995.
27. Pearse DD, Pereira FC, Marcillo AE, Bates ML, Berrocal YA, Filbin MT, Bunge MB: cAMP and Schwann cells promote axonal growth and functional recovery after spinal cord injury. **Nat Med** 10:610–616, 2004.
28. Schwab ME: Repairing the injured spinal cord. **Science** 295:1029–1031, 2002.
29. Song J, Saiz E, Bertozzi CR: A new approach to mineralization of biocompatible hydrogel scaffolds: An efficient process toward 3-dimensional bonelike composites. **J Am Chem Soc** 125:1236–1243, 2003.
30. Stoodley MA, Brown SA, Brown CJ, Jones NR: Arterial pulsation-dependent perivascular cerebrospinal fluid flow into the central canal in the sheep spinal cord. **J Neurosurg** 86:686–693, 1997.
31. Stoodley MA, Gutschmidt B, Jones NR: Cerebrospinal fluid flow in an animal model of noncommunicating syringomyelia. **J Neurosurg** 44:1065–1075, 1999.
32. Tsai EC, Dalton PD, Shoichet MS, Tator CH: Synthetic hydrogel guidance channels facilitate regeneration of adult rat brainstem motor axons after complete spinal cord transection. **J Neurotrauma** 21:789–804, 2004.
33. Tsai EC, van Bendegem RL, Hwang SW, Tator CH: A novel method for simultaneous anterograde and retrograde labeling of spinal cord motor tracts in the same animal. **J Histochem Cytochem** 49:1111–1122, 2001.
34. Weidner N, Ner A, Salimi N, Tuszynski MH: Spontaneous corticospinal axonal plasticity and functional recovery after adult central nervous system injury. **Proc Natl Acad Sci U S A** 98:3513–3518, 2001.
35. Xu XM, Zhang SX, Li H, Aebischer P, Bunge MB: Regrowth of axons into the distal spinal cord through a Schwann-cell-seeded mini-channel implanted into hemisected adult rat spinal cord. **Eur J Neurosci** 11:1723–1740, 1999.

Acknowledgments

We thank Rita van Bendegem, Maria Jimenez-Hamann, Ph.D., William Chung, M.A.Sc., Thomas Freier, Ph.D., and Peter Poon for their excellent technical assistance and Cindi Morshead, Ph.D. for insightful discussion. This work was supported by a Grant-in-Aid from the Ontario Neurotrauma Foundation (Fellowship grant # 2004-SCI-FS-28 awarded to HN), the Natural Sciences and Engineering Research Council of Canada (Strategic grant to MSS and CHT), and by operating funds from the Canadian Paraplegic Association (Ontario Branch).

COMMENTS

Nomura et al. have produced yet another quality research publication addressing spinal cord regeneration. This research arena has been plagued by suboptimal success, dead end research pathways, and suboptimal correlations between laboratory and clinical results. Nevertheless, the Toronto team has persisted. This article is reflective of the difficulties associated with determining the "solution" to the problem, as well as the benefits of using a multimodality approach (e.g., structural conduits and humoral adjuncts) and the benefits associated with persistence and patience. The road to success is long and uncertain, yet this team is appropriately approaching the problem one path at a time.

Edward C. Benzel
Cleveland, Ohio

This is a thorough investigation of a synthetic hydrogel channel used as a scaffold to bridge the gap after spinal cord transection. In a previous study, the authors had demonstrated promotion of regeneration and some functional recovery using synthetic channels in a rat model of spinal cord transection, but had experienced problems with collapse of the channels. In this study, they used reinforced channels with coils lining the inner wall. Although the study was successful in that the channels did not collapse, regeneration was not as pronounced as in the previous study. This was attributed to the formation of syrinxes in the rostral spinal cord stump, which seemed to push the rostral stump caudally.

The cause of syrinx formation in this study is not clear. In addition to the use of a different channel, the animals also received a cocktail of autologous peripheral nerve grafts and acidic fibroblast growth factor. It is not clear from this study whether the syrinxes formed as an expansion of the central canal or as an expansion of a necrotic cyst forming at the site of injury. In either case, it is likely that a perturbation of cerebrospinal fluid flow was at least a contributing factor. The dura was opened widely to insert the channel and was covered with a synthetic graft. It is likely that the dura did not reform completely and that the subarachnoid space became obliterated at the site of the injury. The more robust channel or the nerve growth cocktail could contribute to this obstruction, perhaps by promoting more scar formation. It would be interesting to study cerebrospinal fluid flow in this model to determine whether there is a complete blockage.

There are many promising results from this study and the authors' previous work, including an improvement in functional recovery, evidence of cellular proliferation and formation of myelin in the bridge between the cord stumps, and axonal regeneration (in the previous study). This article has provided important new insights into the use of hydrogel channels in spinal cord injury. Future work will need to take into account spinal cerebrospinal fluid flow at the level of the injury so that syrinx formation is prevented.

Marcus A. Stoodley
Randwick, Australia

Tubular channels may aid spinal cord regeneration after transaction, but they are prone to collapse with the passage of time. Nomura et al. have created and tested novel channels specifically designed to avoid collapse. The authors reported that the utilization of these new channels in a rat model did not result in any improvement in axonal regeneration or functional recovery. A significant number of the animals developed syringomyelia and experienced caudal migration of the rostral stump. These unexpected complications are discussed in detail. The authors are to be congratulated for their honest appraisal of this promising technology and their continuing work in this area.

Vincent C. Traynelis
Iowa City, Iowa

Ever since it was reported that axons grew across a severed thoracic spinal cord through nerve grafts interposed between the rostral and distal stumps, and that some hand limb motion was restored, neuroscientists have tried to replicate this finding. Hydrogel channels for enclosing the nerve grafts have been used by Nomura et al. in previous studies. In the present study, in an attempt to get better regeneration, they used a more rigid tube, but found that the results were not as good as when they used a less rigid channel. Although this paper reports a negative result, there is much valuable information in it for researchers who are attempting to bridge the injured spinal cord.

Robert G. Grossman
Houston, Texas